Scientific Research Publishing

Modeling and Numerical Simulation of Material Science, 2023, 13, 11-27
https://www.scirp.org/journal/mnsms
ISSN Online: 2164-5353
ISSN Print: 2164-5345

Predicting the Volume Fraction of Martensite in Welded Mild Steel Joint Reinforced with Titanium Alloy Powder

Alain Ngenzi[1*], Stephen A. Akinlabi[2], Anthony K. Muchiri[3]

[1]Pan African University Institute for Basic Sciences, Technology and Innovation (PAUSTI), Nairobi, Kenya
[2]Department of Mechanical and Construction Engineering, Northumbria University, Newcastle, UK
[3]Department of Mechatronic Engineering, Jomo Kenyatta University of Agriculture and Technology (JKUAT), Nairobi, Kenya
Email: *alain.ngenzi@students.jkuat.ac.ke

How to cite this paper: Ngenzi, A., Akinlabi, S.A. and Muchiri, A.K. (2023) Predicting the Volume Fraction of Martensite in Welded Mild Steel Joint Reinforced with Titanium Alloy Powder. *Modeling and Numerical Simulation of Material Science*, **13**, 11-27.
https://doi.org/10.4236/mnsms.2023.132002

Received: April 1, 2023
Accepted: April 27, 2023
Published: April 30, 2023

Copyright © 2023 by author(s) and Scientific Research Publishing Inc.
This work is licensed under the Creative Commons Attribution International License (CC BY 4.0).
http://creativecommons.org/licenses/by/4.0/

Open Access

Abstract

Welded mild steel is used in different applications in engineering. To strengthen the joint, the weld can be reinforced by adding titanium alloy powder to the joint. This results in the formation of incomplete martensite in a welded joint. The incomplete martensite affects mechanical properties. Therefore, this study aims to predict the volume fraction of martensite in reinforced butt welded joints to understand complex phenomena during microstructure formation. To do so, a combination of the finite element method to predict temperature history, and the Koistinen and Marburger equation, were used to predict the volume fraction of martensite. The martensite start temperature was calculated using chemical elements obtained from the dilution-based mixture rule. The curve shape of martensite evolution was observed to be relatively linear due to the small quantity of martensite volume fraction. The simulated result correlated with experimental work documented in the literature. The model can be used in other powder addition techniques where the martensite can be observed in the final microstructure.

Keywords

Finite Element Analysis, Martensite Volume Fraction, Dilution, Koistinen and Marburger Equation

1. Introduction

Mild steel's excellent malleability and weldability make it popular for various applications such as cookware, machine parts, and construction [1]. Welding mild steels can have some processing irregularities that need analysis. A weak

zone of the welded joint is often observed because heat makes the welded area undergo microstructural change [2]. Studies related to the strength of the forming joint of material during welding have become an area of interest. Consequently, many methods have been proposed to strengthen steel joints, including metal powder addition in welding [3]. Often, the execution of this method is to use the metal powder, which has mostly different chemical compositions with base metal, as reinforcement, filled into the groove, and a heat source is applied to form the joint. In addition to that, the heat can be provided by the conventional arc welding technique, particularly Gas Metal Arc Welding (GMAW) [3]. The final microstructure phases are obtained at the joint, using the metal addition in welding, depending on the chemical element of metal powder and the base metal. For example, it was shown that welding mild steel reinforced with titanium alloy powder in the joint using GMAW resulted in the formation of the intermetallic compound and martensite phases in the final microstructure [4]. It was due to the mismatch in the chemical composition of base metals and the reinforced powder. The intermetallic compound and martensite phase in the joint have been experimentally investigated in the dissimilar joint. Kumar and Balasubramanian [5] noted that the martensite and intermetallic compound lower the strength of the joint between stainless steel and titanium. In addition, Nikulina *et al.* [6] showed that the martensite formation in the welded dissimilar joint between high-carbon steel and chrome-nickel steel could give rise to failure through fatigue cracking. It is because of the high dislocation density and residual stresses that characterize the martensite.

As the experimental work consumes time and is expensive, numerical methods have been developed to predict the formation of the martensite phase when there is a mismatch of chemical composition in the joint. Esfahani *et al.* [7] predicted the martensite volume fraction in the dissimilar joint formed between the carbon steel and austenitic stainless using the Schaeffler diagram. The martensite phase was also observed by Prabakaran *et al.* [8] using the Schaeffler diagram after welding the AISI 1018 low alloy steel and AISI 316 austenitic stainless steel sheet. On the other hand, Sun *et al.* [9] predicted the volume fraction of martensite in three passes of welding for low alloy steel plate and the SD3 steel as electrode using the dilution-based mixture rule and the Koistinen and Marburger (KM) equation. Dupont and Kusko [10] applied the dilution base mixture rule to predict the martensite start temperature to understand the martensite formation in austenite to ferrite dissimilar welds considering separately the chemical compositions of the nickel-based electrode. Sun *et al.* [9] developed a thermal metallurgical and mechanical model to analysis the effect of the tempering on the microstructure, hardness and residual stress on the joint. The materials used to form the weldment were SA508 Cr.3 Cl.1 steel and S3 and SDX wire steels for base metal and filler respectively. The martensite volume fraction was predicted using the dilution-based mixture rule. From those numerical analyses, the Schaeffler diagram has the limitation of not considering the nitrogen pickup, which sometimes occurs in GMAW [11]. Still, an alternative to this may be the

dilution-based mixture rule.

From the literature, it has been seen that there are still limitations on work that deals with predicting the martensite on the reinforced joint; therefore, the present paper focuses on predicting the volume fraction of martensite in welded steel joint reinforced with titanium alloy powder. First, the thermal transient is simulated to predict the temperature history at the welded zone, Barbier's equation for determining martensite start temperature (M_s) is adopted, and the dilution effect is considered so that the new chemical element can be determined. Secondly, the KM equation is used to determine the volume fraction of martensite. The contribution of this study is to understand the impact of adding titanium alloy powder in the mild steel groove in predicting the martensite phase.

2. Methodology

2.1. Finite Element Analysis

Thermal analysis simulation during the GMAW welding process necessitates three-dimensional modeling. The ANSYS non-linear finite element code is used in this context due to its modeling flexibility and ability to obtain full field numerical solutions. The moving heat source, written in APDL command language, has been inputted for analysis runs. The following sections are steps of finite element method.

2.1.1. Governing Equation and Heat Source Model

To calculate the temperature history, the researchers employed Fourier's equation for three-dimensional heat conduction [12]. This equation is a partial differential equation that includes temperature-dependent material properties and can be expressed as follows:

$$k\frac{\delta^2 T}{\delta x^2}+k\frac{\delta^2 T}{\delta y^2}+k\frac{\delta^2 T}{\delta z^2}+\frac{\delta Q}{\delta t}=\rho C\frac{\delta T}{\delta t} \tag{2.1}$$

The equation above includes several variables and coefficients. The variable Q represents the volumetric internal energy generation, while T represents temperature. The spatial coordinates are denoted by x, y, and z, and time is represented by t. Additionally, the equation incorporates several coefficients: ρ represents the density of the material, C represents specific heat, and k represents the thermal conductivity coefficient.

During welding, the electrode is moving along a direction. Therefore a moving heat source has to be employed. The modified Gaussian heat source model, which its frame is represented by the Gaussian function shown in **Figure 1** is adopted and it is used to simulate the thermal history at different points along the welded zone [13].

$$Q_s(x,y,t)=\frac{3q_s}{\pi r_0^2}\mathrm{e}^{\left(-3\frac{r^2}{d_0^2}\right)} \tag{2.2}$$

Q denotes the rate of heat input. The effective radius of the welding arc is

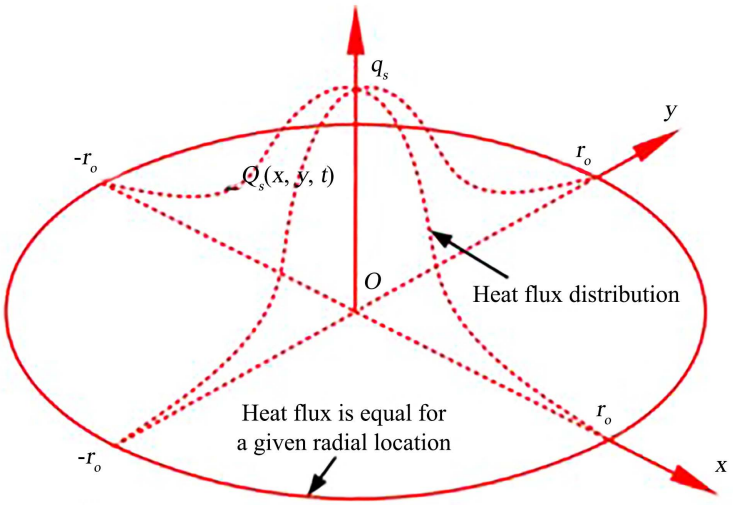

Figure 1. Gaussian heat source model [14].

represented by r_0, and the diameter of the welding arc is represented by d_0. r is calculated by:

$$r = \left(x - x_0\right)^2 + \left(y - vt - y_0\right)^2 \tag{2.3}$$

where x_0 and y_0 represent the distance of the heat source from the reference coordinate system's origin along the x- and y-axes, respectively. The welding arc travel speed is given by v, and the travel time is given by t.

2.1.2. Mesh

In this analysis, the geometrical model was divided into two parts and the hexahedral element was used. The first part is the fusion zone and its surrounding area. The second is for the rest of the area where no high temperature occurred (see **Figure 3**). Due to the high temperature subjected to the first area, a mesh convergence study is based on the maximum temperature attained after the simulation process at a node. The node located 7 mm from the origin along the reinforced welded joint (see **Figure 6**) was chosen for the mesh convergence study. Different maximum temperatures were obtained in the simulation as the mesh size was varied. As the size kept varying, the maximum temperature became constant, as is shown in **Figure 2**. Subsequently, the mesh size of 0.8 mm was chosen to reduce the computational time taken during the simulation. From the mesh convergence results, the first area was sized 0.8 mm, and the remaining area was sized 3 mm. The geometrical model was discretized into 18,072 elements and 90,730 nodes (see **Figure 3**).

2.1.3. Boundary Conditions

Boundary conditions specify the relationship between the domain and the external environment. In welding, boundary conditions are the external specific heat flux which is applied on the top of the specimen and heat losses due to radiation and convection are applied at all faces of the specimen. Each boundary can be described with mathematical description of thermal boundary conditions.

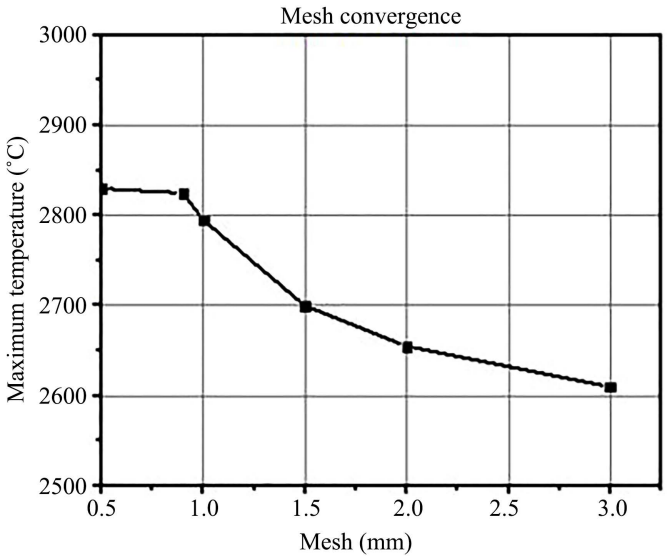

Figure 2. Mesh convergence.

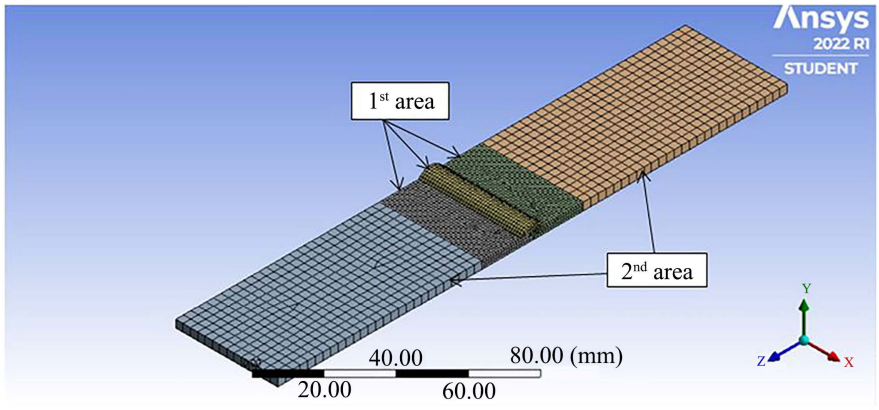

Figure 3. Discretized geometrical model.

The specific heat flux was considered to be Modified Gaussian heat source model discussed in previous section. The equation for convection q_c and radiation q_e are written as [15]:

$$q_c = h \cdot \left(T - T_0\right) \tag{2.4}$$

$$q_e = \dot{\varepsilon} \cdot \xi \cdot \left(T^4 - T_0^4\right) \tag{2.5}$$

The temperature of the room is denoted as T_0, while the convection coefficient and emissivity coefficient for all surfaces of the plate are represented by h and ε, respectively. ξ is the Stefan Boltzmann constant. In thermal analysis, thermal material properties also called the temperature-dependent material properties contribute to the distribution of temperature during the welding process. Those properties are density, thermal conductivity, and specific heat. As each material has their thermal property, **Table 1** shows the properties of mild steel, and **Table 2** shows that titanium alloy powder was considered to be the

same material properties of Ti-6Al-4V. The thermal properties of the electrode were considered to be the same as mild steel because they have small differences in chemical composition. The ANSYS workbench solver did the interpolation to determine the intermediate values of the two tables.

Table 1. Thermal properties for mild steel [16].

T(˚C)	Specific Heat (J/KgC)	Thermal Conductivity (W/mC)	Density (Kg/m^3)
0	480	60	7880
100	500	50	7880
200	520	45	7800
400	650	38	7760
600	750	30	7600
800	1000	25	7520
1000	1200	26	7390
1200	1400	28	7300
1400	1600	37	7250
1550	1700	37	7180

Table 2. Thermal properties for titanium alloy powder [17].

T(˚C)	Density (g/cm^3)	Specific Heat (J/gK)	Thermal Conductivity (W/mK)
25	4.43	0.523	7.7
100	4.41	0.552	7.6
300	4.37	0.623	7.2
500	4.33	0.718	6.6
700	4.29	0.841	5.9
900	4.24	0.998	5.2
1100	4.18	1.193	4.4
1300	4.12	1.432	3.6
1500	4.05	1.727	2.8
1700	3.97	2.087	2
1900	3.88	2.523	1.4
2000	3.84	2.773	1.1
2200	3.74	3.315	0.8
2400	3.63	3.945	0.6
2600	3.51	4.665	0.4
2800	3.38	5.475	0.3
3000	3.24	6.375	0.2

2.2. Formation of Martensite

Phase Transformation

In low-carbon steel, the final microstructure is formed when the temperature is starting to cool down from the austenite finish temperature. From that period, the ferrite phase occurs in different types. First, the allotriomorphic ferrite occurs in the austenite boundary, and as the temperature keeps cooling down, the Widmanstatten ferrite forms. The ferrite formation period is usually in the range of 800˚C to 500˚C [18]. If retained austenite is remained, it becomes either bainite or martensite. When titanium alloy is added to the groove, the titanium particle reacts with the iron particles and forms the intermetallic compound. The presence of titanium alloy powder can lead to the creation of titanium carbide, which then influences the formation of the martensite phase in the welded zone [19]. Considering that the intermetallic and martensite phase cannot be predicted using the same model, this paper only concentrates on predicting the martensite phase occurring in a reinforced butt joint.

The martensite phase transformation is diffusionless, which may occur in non-isothermal phenomena such as welding. The martensite formation can start when the cooling temperature is below the M_s and end at a martensite finish temperature (M_f). Usually, the Ms can vary below 500˚C, and the M_f can even go to room temperature or below. In addition to that, in case the M_s is more than 400˚C, the M_f would be located above the ambient temperature [20].

The formation of martensite can then be modeled by Koistinen and Marburger (KM) equation [21]. The disadvantage of this model is the parabolic shape during the evolution of martensite [22]. The equation is written as follow:

$$V_M = 1 - \exp\left[-A_m \cdot \left(M_s - T\right)\right] \tag{2.6}$$

where V_M is the volume fraction of martensite, M_s is the martensite start temperature, T is temperature, A_m is the constant rate. The value of the constant rate depends on the type of steel. In low-carbon steel, the value is usually equal to 0.011 [23].

It was found that the M_s varies with the chemical composition of materials. For that reason, many researchers have developed different regression models to predict the M_s base on the chemical composition of the material. Considering that the titanium may affect the Ms, the equation employed has to consider the titanium for determining M_s. Barbier [24] created a model that can be used to determine the M_s. Barbier's equation is written as following:

$$\begin{aligned} M_s = {} & 545 - 601.2^{*}\left(1 - \exp\left(-0.868^{*}\mathrm{C}\%\right)\right) - 34.4^{*}\mathrm{Mn}\% - 13.7\mathrm{Si}\% \\ & - 9.2\mathrm{Cr}\% - 17.3\mathrm{Ni}\% - 15.4\mathrm{Mo}\% + 10.8\mathrm{V}\% + 4.7\mathrm{Co}\% \\ & - 1.4\mathrm{Al}\% - 16.3\mathrm{Cu}\% - 361\mathrm{Nb}\% - 2.44\mathrm{Ti}\% - 3448\mathrm{B}\% \end{aligned} \tag{2.7}$$

where C, Mn, Si, Cr, Mo, V, Co, Al, Cu, Nb, Ti, and B are values of weight percentage for each chemical composition on **Table 3** was taken from literature [4].

Table 3. Chemical composition of titanium alloy, mild steel and due elements to dilution.

Elements	Ti alloy (*W*%)	Mild steel (*W*%)	New elements due to dilution (*W*%)
C	-	0.072	0.069
Si	0.32	0.068	0.078
Mn	-	0.32	0.08
P	-	0.0098	-
S	-	0.0091	-
Cr	0.04	0.042	0.042
Mo	3.26	0.0050	1.35
Ni	-	0.0064	0.006
Al	6.20	0.042	0.28
Ti	87.94	-	3.5
Zr	2.17	-	-
Sn	0.7	-	-

It is unreasonable to consider the weight percentage of only the chemical composition of the base metal, whereas the reinforced particle has different chemical compositions from the mild steel. Therefore the mixing degree of the two metals, so-called dilution, was considered. The dilution helps to determine the new chemical elements in the fusion zone [25]. The dilution calculation assumes a homogeneous mixture between two alloys and that the dilution is constant in the welded zone. The dilution is calculated using Equation (2.8) [26].

$$D = \frac{B}{A+B} * 100 \tag{2.8}$$

where B is the melted cross-sectional area of the reinforcement and base metal and A donates the cross-sectional area where titanium alloy filled as shown in **Figure 4**. In **Figure 4**, the red cross-sectional area was considered for determining the dilution.

To calculate the weight percentage of a new chemical element by considering the effect of dilution, therefore the mixture rule is used, and the equation is written as follows [25]:

$$W = W_B * D + W_A(1-D) \tag{2.9}$$

where D is the dilution; W is the weight percentage of chemical composition; W_B and W_A are the weight percentage of the chemical element in the base metals and titanium alloy powder respectively. Equations (2.8) and (2.9) assume that the loss of material due to evaporation is insignificant. Hence, they cannot be used to predict the behavior of alloying elements that have a high vapor pressure, such as magnesium in aluminum alloys [27].

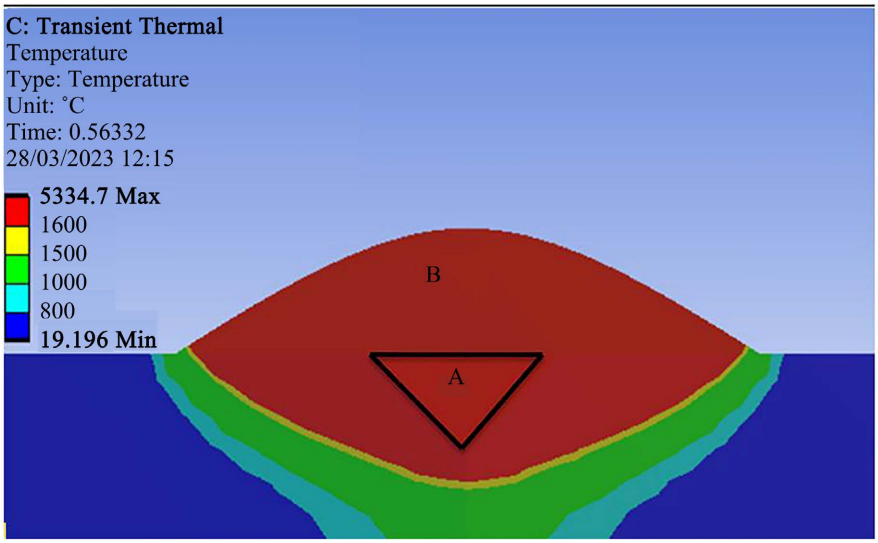

Figure 4. Dilution parameters.

2.3. Thermal Analysis

2.3.1. Weld Pool Geometry

The transient thermal analysis was used to predict the weld pool shape of weldments. The simulated weld pool geometry can be compared to the actual weld geometry obtained through optical microscopy tests to validate the simulation method's effectiveness [28].

To determine the simulated weld pool geometry, a cross-section of the weld joint is cut, and the temperature fields in this cross-section are examined to record the temperature contours [29]. The area where the temperature was above the melting point of mild steel for unreinforced joints and titanium alloy for the reinforced joint was defined as the weld pool geometry.

Figure 5(a) compares the simulation result and experiment result for the unreinforced joint. The red area is for the simulation result, and the white area is for the experiment. The two areas were the weld pool geometry, due to the observed temperature being above the melting point of mild steel, 1430˚C. They were compared to each other and found a good agreement between them. **Figure 5(b)** compares the simulation and experiment results for the reinforced joint. The same areas were identified as it was done in the unreinforced joint by considering the temperature higher than melting point of titanium, 1600˚C. They were also compared to each other and found a good agreement between them. The inaccuracy of the weld bead height shown in those figures is affected by the predetermined bead height used in the simulated model. The bead height was taken as 2 mm.

The dimensions of interest are the depth of penetration and width of the weld pool, measured along the x and y axes of the cross-section. The weld pool is defined as areas with temperatures above titanium's melting point.

Table 4 presents the measured dimensions of the simulated and experimental butt joint geometries, indicating good agreement between the experimental and

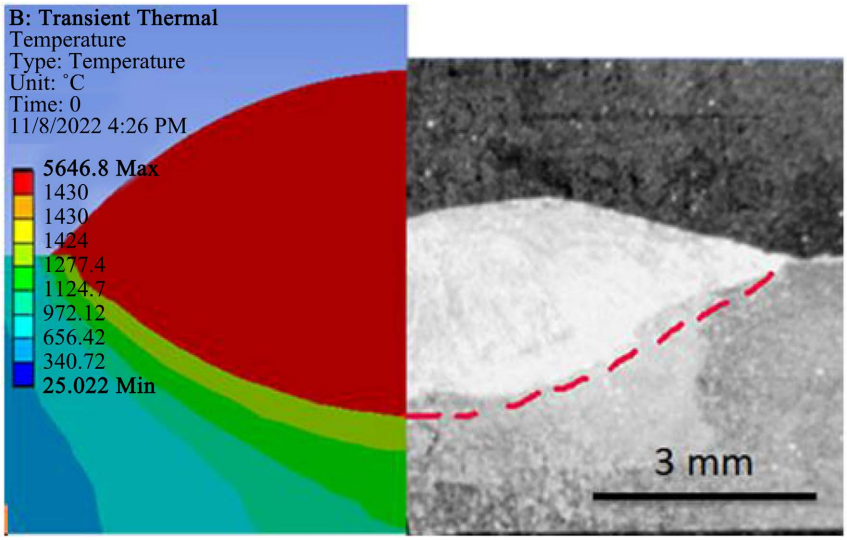

(a)

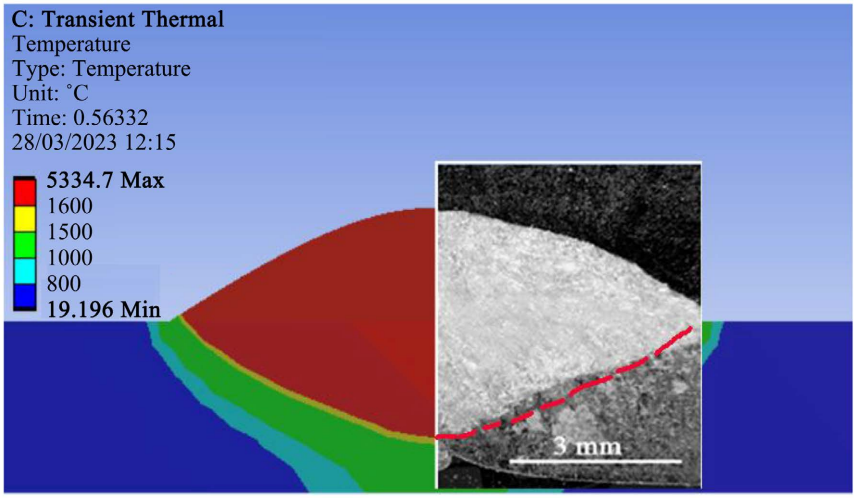

(b)

Figure 5. Comparison simulation result and experimental result. (a) Unreinforced weld pool geometry; (b) Reinforced weld pool.

Table 4. Comparison of weld pool geometry dimensions of unreinforced and reinforced joint from experiment and simulation results.

	Width		Depth penetration	
	unreinforced	reinforced	unreinforced	reinforced
Experimental work (mm)	8.25	9.31	1.65	1.80
Simulation work (mm)	8.22	8.7	1.75	1.98
Relative error (%)	0.3	6	4	10

simulated values for the depth of penetration and the weld pool width. The high relative error was 10%. This error may have occurred because it was challenging to accurately replicate the actual conditions in which the process takes place.

Factors such as material physical parameters may have contributed to the difficulty in matching real conditions [28].

2.3.2. Temperature History

To collect the thermal history in the joint, a temperature probe was inserted at different distances along the weld joint, as shown in **Figure 6**. Thermal history was measured at four different points to observe the variation in temperature in the reinforced welded zone and unreinforced welded joint. In **Figure 8**, the curve shows the peak temperature has been above the melting point of mild steel, 1430˚C. It can be observed that the peak of temperature at each point is different. The observation means that as the welding heat source moves, it causes the heat to transfer from one point to another.

This movement of heat can be observed by the high temperature of the next adjacent node after the previous node has reached its peak temperature. Furthermore, the peak temperature of the next adjacent node is higher than that of the previous one, which suggests that heat is being accumulated. In **Figure 7**, the curve shows that the peak temperature has been above the melting point of titanium alloy powder, 1600˚C. Comparing **Figure 7** and **Figure 8** shows that by adding the titanium inside the groove, the titanium alloy powder slows the cooling. Titanium has a low thermal conductivity, making it retain heat for a long time compared to mild steel. It is observed even in the figures where the cooling rate from 2000˚C to 500˚C was 39.985 s and 41.768 s for unreinforced and reinforced welded joints, respectively.

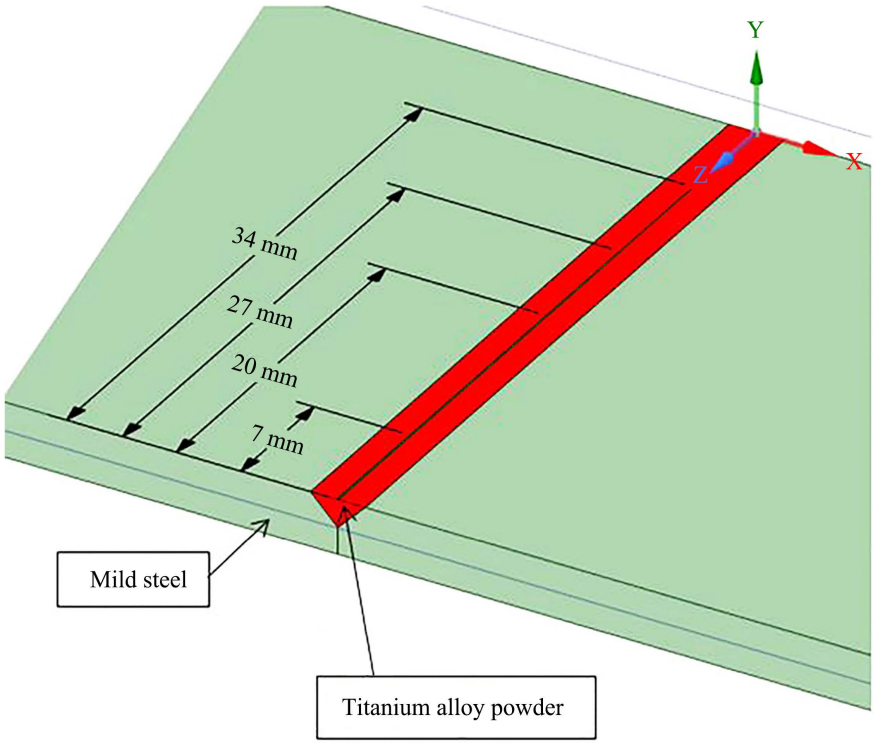

Figure 6. Distances at which the temperature probe was inserted.

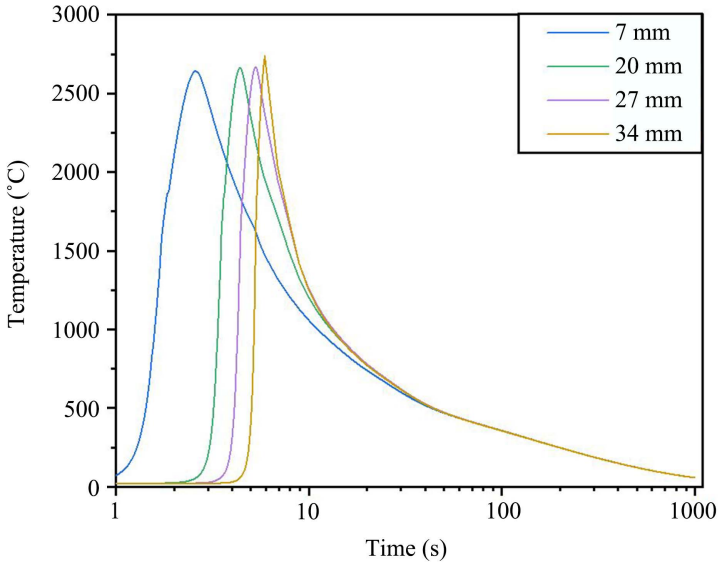

Figure 7. Temperature history at different points along reinforced welded zone.

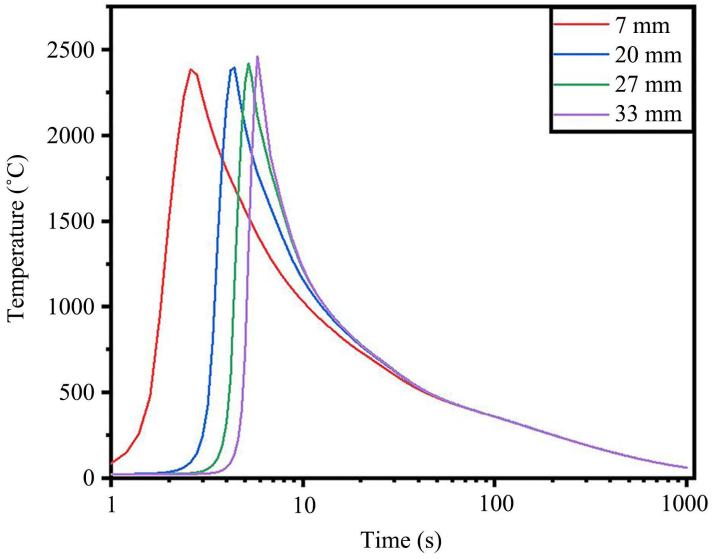

Figure 8. Temperature history at different points along unreinforced welded zone.

2.4. Martensite Phase

The determination of the martensite volume fraction was started by calculating the dilution effect using Equation (2.8). This gave a value of 96%. Then the value was used in Equation (2.9) to determine the new weight percentage of chemical element in the reinforced welded zone, as shown in **Table 3**. The new weight percentage was used to determine the martensite start temperature using Equation (2.7) and the obtained value was 476˚C. The obtained value of M_s can be in agreement with the microstructure observed in optical micrograph. Because, in the microstructure, the lath martensite was observed and this type of martensite starts to form at a high temperature [30]. To finalize the determination of V_M parameters, the temperature was extracted from the thermal history of one point

in the reinforced butt joint. The random choice of the point was because, below the martensite start temperature, the curves of points have the same cooling rate (see also **Figure 7**).

The chosen temperature was employed to simulate the martensite volume fraction. The evolution of martensite volume fraction was plotted in **Figure 9**. The C-shaped curve was expected when the KM equation is used [31]. However, due to a small volume fraction of martensite that was observed in the final microstructure, the curve was quite linear. This was also confirmed by skrotzki [32] who stated that the evolution of martensite volume fraction is quite linear when it is in the range of 6% to 60% of the volume fraction. The course of martensite phase was also in agreement with the work done by Heinze *et al.* [33] who predicted the martensite volume fraction by considering the prior austenite grain size. By Considering **Figure 9**, it is seen that the volume fraction of martensite can be predicted at different temperature. The volume fraction of martensite was 23% in the final microstructure of the reinforced butt joint. The results obtained were compared with the experimental work done by Odiaka *et al.* [4] (see **Table 5**). It was noticed that the difference between experiment and simulation results was 4.2 weight percentages. This may be because of the assumption made on the bead height. It can be concluded that the simulation results correlated with experimental work.

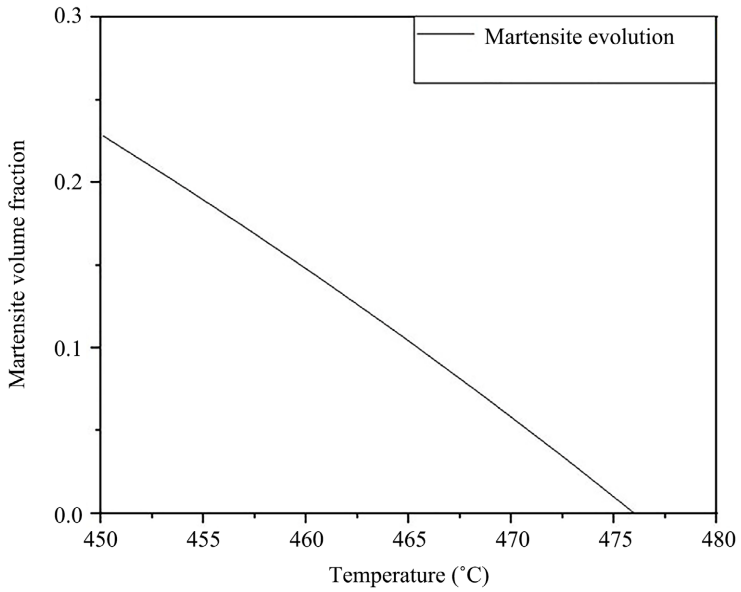

Figure 9. Simulation of volume fraction martensite.

Table 5. Comparison of experimental and simulation result of volume fraction of martensite in reinforced butt welded joint.

	Vol %	
	Experimental result	Simulation result
Reinforced butt joint	18.8	23

3. Conclusion

The present study was to predict the volume fraction of martensite in welded steel butt joint reinforced with titanium alloy powder. The model employed the finite element method to predict the thermal history at the welded joint which acts as driving force on the diffusionless kinetic phase transformation equation, KM equation, to predict the volume fraction of martensite. Dilution base mixture rule was then considered in determining the martensite start temperature. The results obtained were in good agreement with experimental work, with a deviation of 4.2%. This shows that the model can be used in other powder addition techniques where the martensite can be observed in the final microstructure. To increase the accuracy of predicting martensite formation, future research can concentrate on separately utilizing the diverse temperature-dependent material properties of the base metal and filler.

Acknowledgements

The author responsible for the correspondence wishes to express gratitude to the Pan African University, Institute for Basic Sciences, Technology and Innovation (PAUSTI) for their support in conducting this research.

Authors' Contribution

Conceptualization: AN, SAA and AKM, methodology: AN, SAA, and AKM, software: AN, validation AN, SAA, and AKM, data curation AN, formula analysis AN, SAA, and AKM, resources: AN, SAA and AKM, writing original draft preparation: AN, SAA and AKM, writing review and editing AN, supervision: SAA and AKM, project administration AN.

Data Availability

The real data used to illustrate the developed model is within the manuscript.

Conflicts of Interest

The manuscript has been reviewed and approved by all authors for publication in its current form.

References

[1] Kumar, P., Dhingra, A.K. and Kumar, P. (2016) Optimization of Process Parameters for Machining of Mild Steel EN18 by Response Surface Methodology. *Advances in Engineering*: *An International Journal*, **1**, 1-12.

[2] Nia, A.A. and Shirazi, A. (2016) Effects of Different Friction Stir Welding Conditions on the Microstructure and Mechanical Properties of Copper Plates. *International Journal of Minerals*, *Metallurgy*, *and Materials*, **23**, 799-809. https://doi.org/10.1007/s12613-016-1294-0

[3] Odiaka, T., Madushele, N. and Akinlabi, S. (2018) Improvement of Joint Integrity in MIG WELDED STEEL: A Review. *Proceedings of the ASME* 2018 *International Mechanical Engineering Congress and Exposition. Volume* 2: *Advanced Manufac-*

turing, Pennsylvania, 9-15 November 2018.
https://doi.org/10.1115/IMECE2018-86788

[4] Odiaka, T.N., Akinlabi, S.A., Madushele, N., Hassan, S. and Akinlabi, E.T. (2021) Effect of Titanium Alloy Powder Reinforcement on the Mechanical Properties and Microstructural Evolution of GMAW Mild Steel Butt Joints. *Engineering Solid Mechanics*, **9**, 137-152. https://doi.org/10.5267/j.esm.2020.12.005

[5] Kumar, R. and Balasubramanian, M. (2015) Experimental Investigation of Ti-6AL-4V Titanium Alloy and 304L Stainless Steel Friction Welded with Copper Interlayer. *Defence Technology*, **11**, 65-75. https://doi.org/10.1016/j.dt.2014.10.001

[6] Nikulina, A.A., Bataev, A.A., Smirnov, A.I., Popelyukh, A.I., Burov, V.G. and Veselov, S.V. (2015) Microstructure and Fracture Behaviour of Flash Butt Welds between Dissimilar Steels. *Science and Technology of Welding and Joining*, **20**, 138-144. https://doi.org/10.1179/1362171814Y.0000000265

[7] Nekouie Esfahani, M.R., Coupland, J. and Marimuthu, S. (2015) Numerical Simulation and Experimental Investigation of Laser Dissimilar Welding of Carbon Steel and Austenitic Stainless Steel. In Green, M. and Rose, C., Eds., *Industrial Laser Applications Symposium* (*ILAS* 2015), Vol. 9657, SPIE, Bellingham, 172-181.
https://doi.org/10.1117/12.2176026

[8] Prabakaran, M.P., Kannan, G. and Lingadurai, K. (2019) Microstructure and Mechanical Properties of Laser-Welded Dissimilar Joint of AiSi316 Stainless Steel and Aisi1018 Low Alloy Steel. *Caribbean Journal of Science*, **53**, 978-998.

[9] Sun, Y., Hamelin, C.J., Smith, M.C., Vasileiou, A.N., Flint, T.F. and Francis, J.A. (2018) Modelling of Dilution Effects on Microstructure and Residual Stress in a Multipass Weldment. *Proceedings of the ASME* 2018 *Pressure Vessels and Piping Conference*. *Volume* 6*A*: *Materials and Fabrication*, Prague, 15-20 July 2018.
https://doi.org/10.1115/PVP2018-85110

[10] Dupont, J.N. and Kusko, C.S. (2007) Martensite Formation in Austenitic/Ferritic Dissimilar Alloy Welds. *Welding Journal*, **86**, 51-54.

[11] Hathesh, M. (2020) A Review on Welding Related Problems and Remedy of Austenitic Stainless Steels. *International Research Journal of Engineering and Technology* (*IRJET*), **7**, 5166-5174.

[12] Chen, X.J., Xiao, N.M., Li, Z.D., Li, G.Y. and Sun, G.Y. (2014) The Finite Element Analysis of Austenite Decomposition during Continuous Cooling in 22MnB5 Steel. *Modelling and Simulation in Materials Science and Engineering*, **22**, Article ID: 065005. https://doi.org/10.1088/0965-0393/22/6/065005

[13] Timothy, O., Akinlabi, S.A., Madushele, N., Fatoba, O.S., Hassan, S., Mkoko, Z. and Akinlabi, E.T. (2021) Numerical Analysis of Butt and Lap Welded Titanium Reinforced Mild Steel Joints. *Materials Today*: *Proceedings*, **44**, 1175-1184.
https://doi.org/10.1016/j.matpr.2020.11.236

[14] Wang, J.Q., Han, J.M., Domblesky, J.P., Yang, Z.Y., Zhao, Y.X. and Zhang, Q. (2016) Development of a New Combined Heat Source Model for Welding Based on a Polynomial Curve Fit of the Experimental Fusion Line. *The International Journal of Advanced Manufacturing Technology*, **87**, 1985-1997.
https://doi.org/10.1007/s00170-016-8587-3

[15] Tailor, D.H., Srinivasan, K.N., Channiwala, S.A. and Panwala, M.S.M. (2009) Simulation of Temperature Field of TIG Welding Using FDM. *Proceedings of the ASME 2009 Pressure Vessels and Piping Conference*. *Volume* 6: *Materials and Fabrication*, *Parts A and B*, Prague, 26-30 July 2009, 515-521.
https://doi.org/10.1115/PVP2009-77697

[16] Stamenkovic, D. and Vasovic, I. (2009) Finite Element Analysis of Residual Stress in Butt Welding Two Similar Plates. *Scientific Technical Review*, **59**, 57-60.

[17] Titanium Proprietes. Total Materia. https://www.totalmateria.com/page.aspx?ID=titaniumproperties&LN=EN

[18] Zhang, W., Elmer, J.W. and DebRoy, T. (2002) Modeling and Real Time Mapping of Phases during GTA Welding of 1005 Steel. *Materials Science and Engineering*: *A*, **333**, 320-335. https://doi.org/10.1016/S0921-5093(01)01857-3

[19] Frenzel, J., Zhang, Z., Somsen, C., Neuking, K. and Eggeler, G. (2007) Influence of Carbon on Martensitic Phase Transformations in NiTi Shape Memory Alloys. *Acta Materialia*, **55**, 1331-1341. https://doi.org/10.1016/j.actamat.2006.10.006

[20] Feng, Z.Y., Ma, N.S., Tsutsumi, S. and Lu, F.G. (2021) Investigation of the Residual Stress in a Multi-Pass T-Welded Joint Using Low Transformation Temperature Welding Wire. *Materials*, **14**, Article No. 325. https://doi.org/10.3390/ma14020325

[21] Bubnoff, D.V., Carvalho, M.M.O., de Castro, J.A. and Lourenço, T.R.M. (2016) Kinetic Study on Martensite Formation in Steels 1045 and 4340 under Variable Cooling Rates. *Materials Science Forum*, **869**, 550-555. https://doi.org/10.4028/www.scientific.net/MSF.869.550

[22] Napoli, G., Mengaroni, S., Rallini, M., Torre, L. and Di Schino, A. (2017) Analysis of the Effect of Interrupted Quenching on Microstructure of High Carbon Steels for Forgings. *Advanced Materials Proceedings*, **2**, 799-801. https://doi.org/10.5185/amp.2017/995

[23] Santofimia, M.J., Van Bohemen, S.M.C. and Sietsma, J. (2013) Combining Bainite and Martensite in Steel Microstructures for Light Weight Applications. *Journal of the Southern African Institute of Mining and Metallurgy*, **113**, 143-148.

[24] Barbier, D. (2014) Extension of the Martensite Transformation Temperature Relation to Larger Alloying Elements and Contents. *Advanced Engineering Materials*, **16**, 122-127. https://doi.org/10.1002/adem.201300116

[25] Sun, Y.L., Obasi, G., Hamelin, C.J., Vasileiou, A.N., Flint, T.F., Balakrishnan, J., Smith, M.C. and Francis, J.A. (2019) Effects of Dilution on Alloy Content and Microstructure in Multi-Pass Steel Welds. *Journal of Materials Processing Technology*, **265**, 71-86. https://doi.org/10.1016/j.jmatprotec.2018.09.037

[26] Jindal, S., Chhibber, R. and Mehta, N.P. (2015) Prediction of Element Transfer due to Flux and Optimization of Chemical Composition and Mechanical Properties in High-Strength Low-Alloy Steel Weld. *Proceedings of the Institution of Mechanical Engineers*, *Part B*: *Journal of Engineering Manufacture*, **229**, 785-801. https://doi.org/10.1177/0954405414531113

[27] DuPont, J.N. and Marder, A.R. (1996) Dilution in Single Pass Arc Welds. *Metallurgical and Materials Transactions B*, **27**, 481-489. https://doi.org/10.1007/BF02914913

[28] Sun, G.F., Wang, Z.D., Lu, Y., Zhou, R., Ni, Z.H., Gu, X. and Wang, Z.G. (2018) Numerical and Experimental Investigation of Thermal Field and Residual Stress in Laser-MIG Hybrid Welded NV E690 Steel Plates. *Journal of Manufacturing Processes*, **34**, 106-120. https://doi.org/10.1016/j.jmapro.2018.05.023

[29] Piekarska, W. and Kubiak, M. (2011) Three-Dimensional Model for Numerical Analysis of Thermal Phenomena in Laser-Arc Hybrid Welding Process. *International Journal of Heat and Mass Transfer*, **54**, 4966-4974. https://doi.org/10.1016/j.ijheatmasstransfer.2011.07.010

[30] Maki, T. (2012) Morphology and Substructure of Martensite in Steels. In: Pereloma, E. and Edmonds, D.V., Eds., *Phase Transformations in Steels*, Woodhead Publish-

ing, Sawston, 34-58. https://doi.org/10.1533/9780857096111.1.34

[31] Lee, S.-J. and Van Tyne, C.J. (2012) A Kinetics Model for Martensite Transformation in Plain Carbon and Low-Alloyed Steels. *Metallurgical and Materials Transactions A*, **43**, 422-427. https://doi.org/10.1007/s11661-011-0872-z

[32] Skrotzki, B. (1991) The Course of the Volume Fraction of Martensite vs. Temperature Function $M_x(T)$. *Le Journal de Physique IV*, **1**, C4-367-C4-372. https://doi.org/10.1051/jp4:1991455

[33] Heinze, C., Pittner, A., Rethmeier, M. and Babu, S.S. (2013) Dependency of Martensite Start Temperature on Prior Austenite Grain Size and Its Influence on Welding-Induced Residual Stresses. *Computational Materials Science*, **69**, 251-260. https://doi.org/10.1016/j.commatsci.2012.11.058